Wear 510–511 (2022) 204507

Contents lists available at ScienceDirect

Wear

journal homepage: www.elsevier.com/locate/wear

Tribo-induced surface deformation mechanisms govern friction and wear in ultra-light HCP and duplex Mg–Li alloys

Yue Yang, Ao Meng, Xiang Chen *, Yonghao Zhao **

Nano and Heterogeneous Materials Center, School of Materials Science and Engineering, Nanjing University of Science and Technology, Nanjing, 210094, China

ARTICLE INFO

Keywords:
Magnesium alloys
Friction
Nanostructure
Dynamic recrystallization

ABSTRACT

Adding lithium into Mg can activate more deformation modes in both hexagonal close packed (hcp) and body centered cubic (bcc) Mg–Li alloys. In this work, friction and wear tests were performed on coarse-grained Mg-xLi-3Al–3Zn (x = 4 and 10 wt %) alloys and detailed surface deformation mechanisms were uncovered. Compared with the duplex Mg–10Li alloy, the hcp Mg–4Li shows a 40% lower friction coefficient and a significantly smaller wear rate by nearly one order of magnitude. The low wear rate stems from formation of hard and stable nanograined surface layer through rapid grain refinement of the hcp grains upon sliding. While for the dual-phase alloy, dynamic recrystallization (DRX) dominates the deformation of bcc grains, unavoidably causing its cracking and delamination within the ultra-fine grained DRX layer. Our results are suggestive in designing wear resistant ultra-light Mg–Li alloys through in-depth understanding of tribo-induced surface deformation mechanisms.

1. Introduction

As the lightest structural materials, magnesium-lithium (Mg–Li) alloys are highly attractive in the industrial fields where light weight is critical [1]. As well established in the phase diagram, the matrix transits from the single α-Mg phase (0–5.7 wt% Li) with a hexagonal close-packed (hcp) crystal structure to a duplex structure of both hcp α-Mg phase and body-centered cubic (bcc) structure β-Li phase (5.7–10.3 wt% Li) [2,3]. The α-Mg phase has a moderate strength and a poor formability because of the limited slip systems, while the β-Li phase with bcc structure is more soft and ductile due to the activation of a higher number of slip systems [4]. Coexistence of α-Mg phase and β-Li phase is supposed to induce a balanced ductility and moderate strength.

Bulk deformation of hcp and duplex Mg–Li alloys reckons on basal slip and twinning at room temperature. The addition of Li content could diminish the axial ratio (c/a) of α-Mg phase, thereby lowering critical resolved shear stresses (CRSSs) of slip systems and activating more deformation modes [5]. This is substantiated by the fact that prismatic slip took a paramount role at the initial stage of deformation in the extruded Mg–4Li alloy at room temperature [6]. For the duplex Mg–8Li alloy under monotonic compression and tension loading, the basal <a> slip and pyramidal <a> slip ensured the smooth plastic deformation of α-Mg phase. On the other hand, dynamic recrystallization (DRX) was frequently observed in the soft β-Li phase under deformed condition [7]. In the Mg-9.15Li alloy under hot compression, DRX was easily captured in β-Li phase but retarded in α-Mg phase [8]. The bulk deformation discrepancy between the hcp and duplex phases is intimately correlated to the different asymmetry nature of the crystal structure and critical resolved shear stress of active deformation modes.

Friction-induced surface deformation is distinctly different from bulk deformation as large plastic strains and strain gradient are involved in the confined contacting areas, which undoubtedly affects the tribological performance [9–11]. Therefore, the tribo-induced surface deformation of Mg–Li alloys must be considered when used in the practical applications such as electronic devices and in the fields of automobile and aerospace. Grain refinement, grain coarsening, DRX and interactions with environments were reported in various Mg alloys during sliding [12,13]. Among them, it was perceived that grain boundary sliding induced softening is considered to be responsible for the elevation of wear rate in Mg–Li alloys [14]. Recently, the fretting wear results showed that duplex Mg–Li–Al based alloys have less wear volume loss and lower coefficient of friction (COF) than conventional AZ31. During the wear process, a combination of adhesion, delamination, abrasion and oxidation wear exerted leading roles [15]. In spite of these attempts,

* Corresponding author.
** Corresponding author.
E-mail addresses: xiang.chen@njust.edu.cn (X. Chen), yhzhao@njust.edu.cn (Y. Zhao).

https://doi.org/10.1016/j.wear.2022.204507
Received 16 June 2022; Received in revised form 28 August 2022; Accepted 15 September 2022
Available online 20 September 2022

the understanding of the correspondence between surface deformation mechanisms and the tribological behaviors is still insufficient, not to mention that the difference between hcp and duplex Mg–Li alloys against friction and wear has never been examined before.

In this study, we choose to investigate the friction and wear difference between hcp and duplex Mg–Li alloys. Our research therefore focuses on tracking their surface morphology changes and subsurface structure evolution, in an attempt to delineate the surface deformation related tribological behaviors in the Mg–Li alloys.

2. Material and methods

Commercially available multi-component Mg-xLi-3Al–3Zn alloys with varying content of Li (4 and 10 wt %) were chosen in this study which are referred to as L4 and L10 alloy. Specimens for scanning electron microscope (SEM) observation were sectioned, polished and then etched for 5–10s with a solution consisting of 6 g picric acid, 5 ml acetic acid, 10 ml distilled water and 100 ml ethanol.

The friction and wear tests were performed by a ball-on-disc facility (UMT-2, Bruker, USA) under dry conditions. Fig. S1 illustrates a schematic diagram of the tribo-system. All the wear tests were conducted at room temperature (~20 °C)in air with a relative humidity of ~32%. The counterpart was a Al_2O_3 ball with 6 mm in diameter. Linear reciprocating motion was produced with a slide stroke of 5 mm, a sliding speed of 5 mm/s and a normal load of 2 N, 5 N and 10 N. The calculated contact pressure is 0.44, 0.60 and 0.76 GPa, respectively. Hence, plastic deformation can be initiated within a thick surface layer upon contact loading so as to investigate the tribological behavior and corresponding surface deformation mechanisms. One sliding cycle equals two strokes. Before wear testing, the samples were ground with silicon carbide paper and finally polished to 0.31 μm Ra. After wear testing, the samples were cleaned in an ultrasonic bath with ethanol for 5–10 min and dried in the air to remove any loose debris. The profiles of the worn surfaces were examined using 3D optical surface profiler so as to calculate the wear volume which was determined by the product of the cross-sectional area and the length of the wear track. For each wear condition, three specimens were tested to ensure the repeatability in data. Worn surface morphologies were also characterized by SEM. The hardness measurements were conducted on worn subsurface of the L4 and L10 alloys by using a G200 Nano Indenter. The buried subsurface structure in these two alloys was characterized by SEM and transmission electron microscope (TEM). TEM specimens were cut at the center of the wear track along the sliding direction in a focused ion beam (FIB) system (Carl Zeiss Auriga).

3. Results and discussion

Consistent with the Mg–Li binary phase diagram, the starting L4 sample consists of α-Mg grains with an average size of about 25 μm (see Fig. 1a). Besides the indexed main phase of α-Mg, a small volume fraction of bright particles is distributed at grain boundaries, which is AlLi phase according to the XRD results (Fig. S2a). The L10 alloy exhibits a duplex microstructure including the long ribbon-like α-Mg phase and the equi-axed β-Li phase. There are two kinds of precipitates in the L10 specimen. Small particles are found in the interior of α-phase and particles of circular shape can be clearly seen in the β-Li phase (Fig. 2b). According to the EDS analysis of circular particles (Fig. S2b), the elemental composition is Mg, Al and small quantity of Zn. As the invisibility of Li in SEM, combined with the results of previous study [16], the particles are determined to be AlLi compound. XRD analysis identified L10 alloy is mainly composed of α-Mg, β-Li, AlLi and $MgLi_2Al$ phases (Fig. S2a). Accordingly, it can be deduced that the small particles in the α-phase are $MgLi_2Al$. Typical engineering stress-strain curves of L4 and L10 alloys are plotted (Fig. S2c). With an increase of Li addition from 4 to 10 wt %, the ultimate tensile strength (UTS) reduces from 277 to 187 MPa. Elongations to failure are ~ 22 and 30%, respectively.

Typical coefficient of friction (COF) variation with the sliding cycles at applied loads of 2, 5 and 10 N are presented in Fig. 1c. COF of all the samples increases instantly upon sliding and reaches a stable value after dozens of cycles, although the fluctuation is still visible. The L4 alloy displays a steady-state COF of ~ 0.30 under all loads, which is 40% lower than that of L10 samples (~ 0.5). Besides, the COF presents a slight downward trend with increasing the applied load. The L4 alloy shows a narrow wear track after 900 cycles (Fig. 1d), in contrast to the wide and deep wear track of the L10 alloy (Fig. 1e). The wear rate of the tested samples as a function of the applied load is calculated by dividing the volume loss by the normal force and sliding distance (Fig. 1f). Obviously, the L4 alloy has a dramatically smaller wear rate as compared to the L10 alloy, corresponding to almost an order of magnitude reduction at all loading circumstances. The measured wear

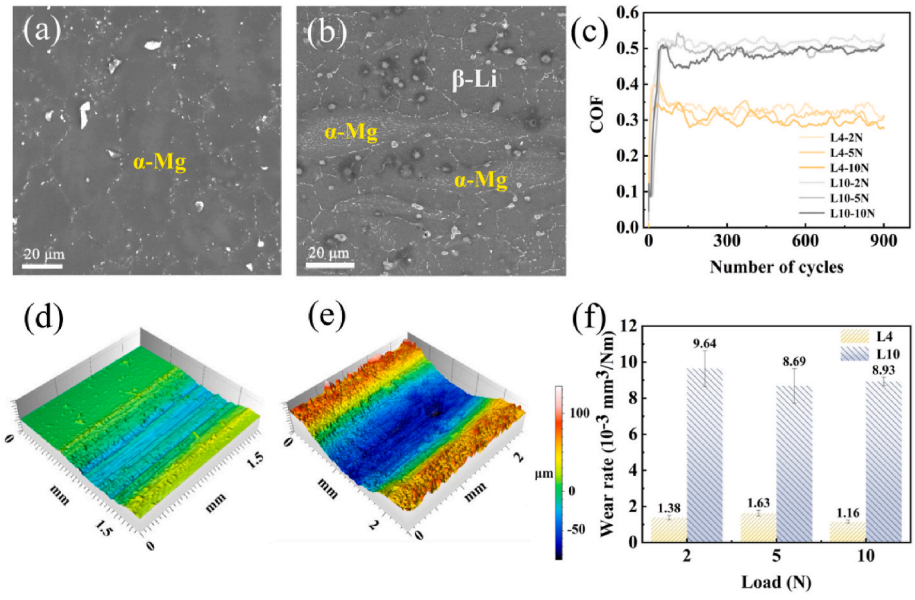

Fig. 1. (a)–(b) typical SEM images of the L4 and L10 alloys; (c) variation of COFs with sliding cycles; (d)–(e) 3-D profile for surface morphologies of the L4 and L10 samples after sliding for 900 cycles under a load of 10 N; (f) wear rate of the L4 and L10 samples after sliding for 900 cycles.

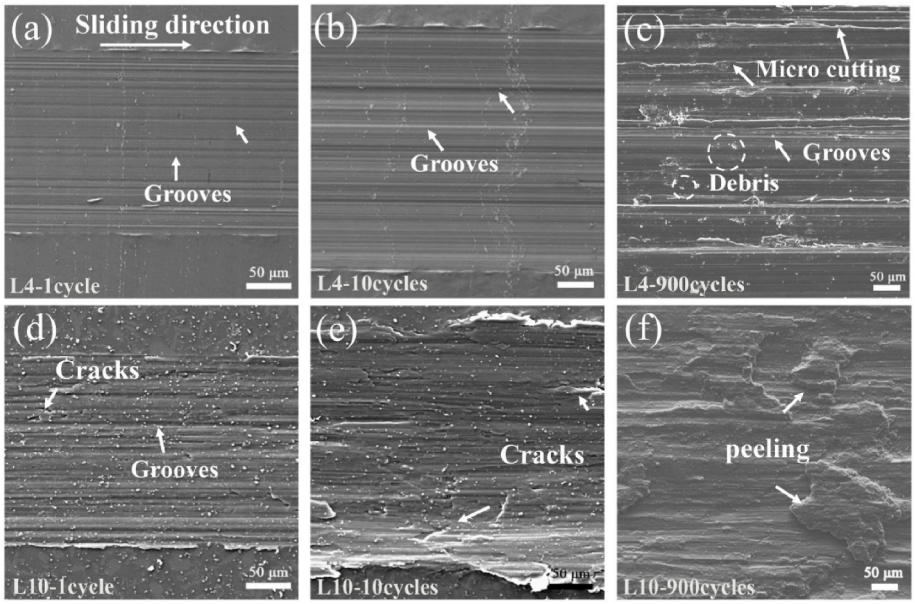

Fig. 2. SEM micrographs for the wear surface of the (a)–(c) L4 and (d)–(f) L10 samples after sliding for 1, 10 and 900 cycles under a load of 10 N.

rate result agrees well with the friction coefficient, illustrating the occurrence of various wear mechanisms during the sliding wear process for the hcp L4 alloy and duplex L10 alloy. Hardly any obvious wear marks can be seen on the surface of the counter bodies in all cases but there is a layer of transfer film (Fig. S3). The surface topographical area scans and representative cross-sectional wear depth plots in Fig. S4 indicate the counter bodies are rarely worn in sliding wear with some materials adhered to the surface. Therefore, it can be determined that the wear rate of the counter bodies can be negligible in this tribo-system.

To unravel the wear mechanisms, the morphologies of the wear surface at the applied load of 10 N at 1, 10, 900 cycles were further investigated using SEM combined with EDS. It can be discernible that the worn surfaces of L4 specimens are covered by numerous grooves along the sliding direction after 1 and 10 cycles, indicating the ploughing mechanism (Fig. 2a and b). With continuous reciprocating sliding, the edge of the grooves becomes sharp and peels off to form wear debris which has the micro-cutting effect (Fig. 2c). It is clear that abrasive wear is the main mechanism and the corresponding sub mechanisms are micro-ploughing and micro-cutting [17]. The L10 samples show a completely different scenario and small cracks occur immediately on the surface after 1 cycle (Fig. 2d). After multiple repeated sliding, large peeling pits and coarse oxide patches are present on the rough worn surface, which is the typical feature of delamination (Fig. 2f). The contact surfaces of the counterpart balls after sliding against each sample for 900 cycles were also examined by EDS (Fig. S5). It can be seen that a substantial amount of magnesium oxides are adhered to the ball surface which hidden the Al element. Therefore, slight adhesive wear occurred in the friction and wear process of the L4 and L10 samples with materials transferred from the body to the counter body. The collected wear debris of both materials was further observed to characterize the wear mechanisms. As shown in Fig. S6, the debris of the L4 samples is tiny and fragmented, whereas the debris in the case of L10 samples has flakes and sheet-like shape, which is generally caused by the initiation and propagation of cracks in the subsurface structure. The EDS analysis of the wear debris in both samples after sliding for 900 cycles under a load of 10 N indicates the presence of magnesium oxides (Fig. S7). The higher amount of oxygen is detected in the debris of the L10 sample. High-concentration O element is also demonstrated on the corresponding worn surface (Fig. S8), indicating the debris was parts of the oxide layer generated by tribochemical reactions that detached after multiple repeated sliding.

Subsurface SEM observations show that high tribological loading induced noticeably refined microstructure in the topmost layers of two alloys. The topmost layer of the L4 sample persists with numerous refined grains and some straight lamellar structures in the adjacent coarse grain interior (Fig. 3a). No cracks are initiated in the subsurface layer. However, large cracks can be obviously observed in the subsurface structure of the L10 sample underneath which α-Mg phase is deformed along the sliding direction (Fig. 3b). Generally, the cyclic contact stresses under multiple sliding result in the crack formation below the surface [18]. As the crack propagates to the surface, delamination occurs to produce thin and long wear debris, leading to the rapid material removal and high wear rate eventually. Thus, delamination on the wear track in the L10 samples is considered to be a sub-mechanism of surface fatigue. The corresponding subsurface micro hardness distributions are compared (Fig. 3c). The hardness of the L4 alloy grows markedly at the depth of 0–20 μm and then gradually decreases to around 0.83 GPa, i.e. the unaltered matrix hardness. Apparently, the hardness of L10 alloy becomes much less at the same depth and the varied trend of hardness value is relatively flat.

The typical TEM images of the topmost tribo-layer of two alloys sliding after 1, 10 and 900 cycles are presented in Fig. 4. Apparently, there is a nanostructured surface layer formed in the worn L4 alloy. The original coarse grains have been refined into randomly oriented nano grains (NGs) within ~ 1 μm depth below the surface after 1 cycle (Fig. 4a). The corresponding selected area electron diffraction (SAED) pattern (Fig. 4g) demonstrates the formation of hcp NGs. The increase of the sliding cycle to 10 leads to a much thicker (~ 5 μm) nanostructured tribo-layer with grain size stabilized below 100 nm. Besides, when the cycle number increases to 900, there exists an about 1 μm thick bright contrast zone composed of plenty of oxygen from the environment, which provides evidence for the existence of mechanical mixing, a sub mechanism of tribo-chemical reactions. The grains beneath the oxide layer experience slight growth (Fig. 4c and Fig. S9). Massive amounts of lamellar structure confirmed as deformation twinning can also be observed underneath the topmost nanostructured layer (Figs. S10d–f).

In sharp contrast to the L4 alloy, the L10 alloy exhibits two types of grains evident in submicron-sized: the first type of grains have irregular grain boundaries and a high dislocation density in the grain interiors, whereas the grain boundaries of the other type are sharp and few dislocations inside the grains. The corresponding SAED pattern shows typical rings of hcp α-Mg and bcc β-Li phases (Fig. 4h). Specifically, some

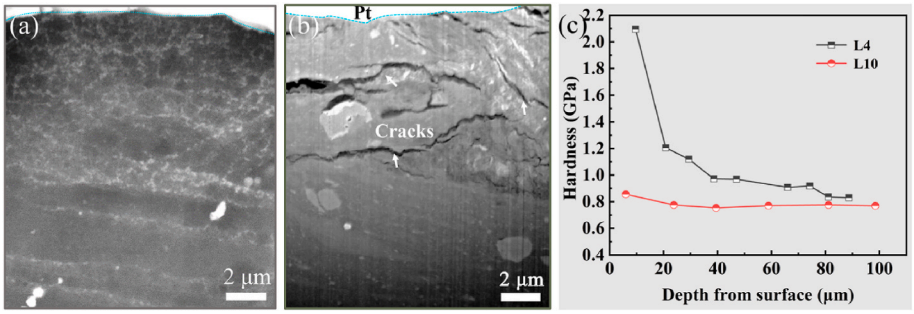

Fig. 3. Typical SEM cross-sectional images of the subsurface layer in the (a) L4 and (b) L10 alloy after sliding for 900 cycles under a load of 10 N; (c) corresponding micro hardness variation along the depth from the surface.

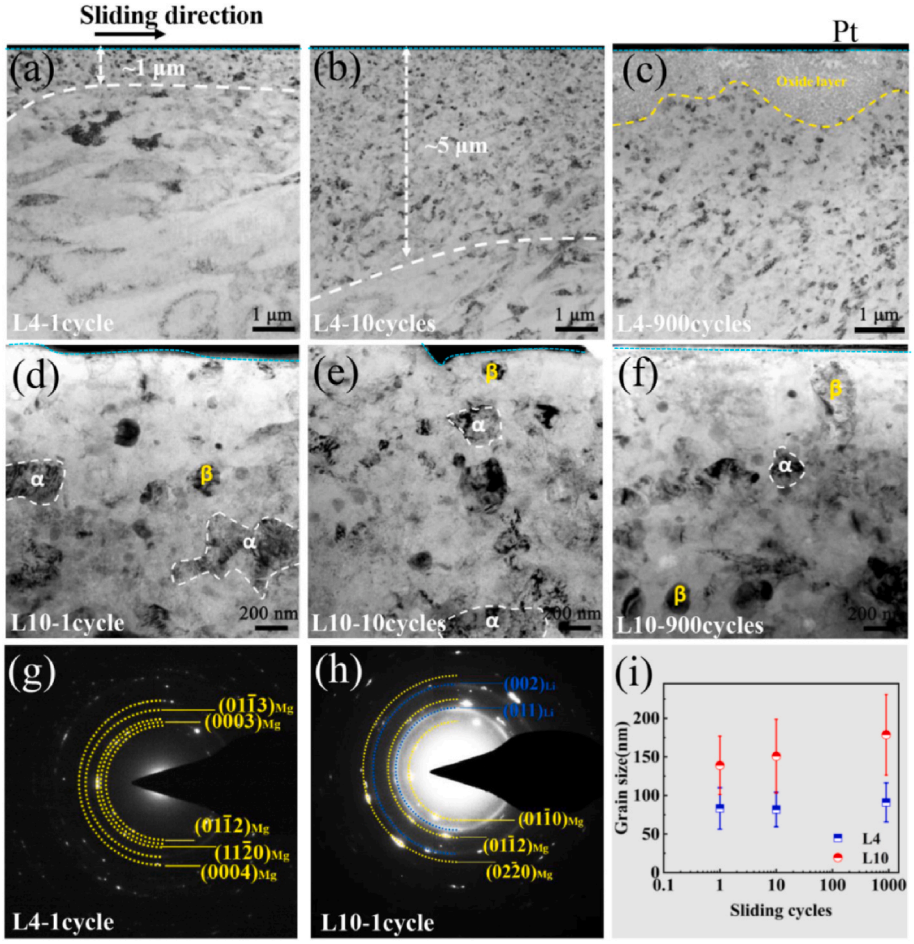

Fig. 4. Typical TEM images of the topmost tribo-layer in the (a)–(c) L4 and (d)–(f) L10 samples after sliding for 1, 10, and 900 cycles under a load of 10 N; (g)–(h) SAED patterns for the topmost tribo-layer in (a) and (d); (i) histogram of grain size distribution of the tribo-layer in the L4 and L10 samples, respectively.

of newly formed grains having sharp grain boundaries appear in the topmost layer after 1 cycle that could be the DRX microstructure [19]. In addition, high density of dislocations is observed inside grains circled with white dotted line (Fig. 4d). The SAED pattern can still show single crystal characteristic of hcp structure, indicating that the grains with irregular grain boundaries in the circled area are α-Mg phase (Fig. S11). Therefore, the DRX microstructure is confirmed to be β-Li phase. As the cycle number increases, the α-Mg phase is further refined, while the grain size of the DRX β-Li phase increases slightly and falls in the range of ~ 200 nm. The average grain size distributions in the topmost tribo-layer of L4 and L10 alloys are statistically shown as a function of the cycle number in Fig. 4i, respectively. The grain size of most NGs in the L4 alloy is between 80 and 90 nm while grains in the L10 alloy are distributed in 130–180 nm.

Our study demonstrates the wear rates for coarse-grained hcp and duplex Mg–Li alloys differ by as much as nearly one order of magnitude. Based on the above analysis and discussion, the wear mechanism for the hcp L4 alloy during reciprocating sliding is dominated by abrasive wear with the corresponding sub mechanisms are micro-ploughing and micro-cutting. The dominant wear mechanisms for the duplex L10 alloy are delamination and oxidation which are generated by surface fatigue and tribochemical reactions, respectively. This unexpected phenomenon can be interpreted from the tribo-induced surface deformation mechanisms of Mg–Li alloys under tribological loading. Obviously, in the hcp L4

alloy after only one cycle, coarse hcp grains have evolved into continuous nanostructured tribo-layer, which is mainly associated with the generation and movement of dislocations caused by the strain accumulation during sliding [20,21]. The measured micro hardness in sub surface after sliding test identifies the strain hardening originating from the nanostructured layer which is beneficial in mitigating friction and wear by a reduced contact area at a fixed stress [22,23]. Furthermore, the L4 samples reveal massive twins in α-Mg grains underneath the tribo-layer, in such a way to withstand high tribological strains. The excess energy of the large amount of twin boundaries is substantially smaller than that of ordinary high-angle grain boundaries, which makes them reluctant to recrystallize [24,25]. Although refining grains to the nanoscale is challenging in bulk deformation of Mg–Li alloys, tribo-induced surface deformation commonly incorporates large plastic strains, strain gradient and even high strain rates, facilitating the formation of nanograins and twins in the confined areas [26,27]. This echoes to a recent publication of the same hcp Mg–4Li alloy deformed by high strain rate rotary swaging. Massive twins and SFs are formed in the grain interior during the swaging process, which are effective in impeding dislocation movement and retaining strain hardening [28].

Surface deformation possesses unique characteristics in the duplex Mg–Li alloy during friction. The β-Li phase is generally thought to be a soft phase, while α-Mg phase is hard. Under the same applied stress, the surface deformation may be transferred to β-Li phase firstly [29]. Phase interfaces could obstruct and limit the movement of dislocations in β-Li phase. As a result, the stored energy of β-Li phase increases, as does the dislocation density at phase boundaries, resulting in a decreased critical strain for DRX [30]. The stress concentration accumulated at some phase boundaries tends to promote the deformation of α-Mg grains as cumulative strain increases. Considering the high proportion (~ 75%) of soft β-Li phase in the L10 alloy, DRX process plays the dominant role in the evolution of microstructure. Owing to the reduced plastic deformation ability of small DRX grains, laminar cracks are generated in the worn subsurface layer, resulting in the rapidly fracture and peeling-off of the topmost layer. Thus, delaminated oxidized layer can be observed on the worn surface. Our previous investigations also confirmed the fine grained DRX layer is brittle during sliding of copper alloys, as the ultra-fine grains hold limited space for dislocation accommodation and work-hardening, making it difficult to accommodate the high accumulated strains in the beginning of sliding [31,32]. Remarkable lower hardness observed in the subsurface layer of L10 alloy proves the softening effect from DRX. Cracking and peeling-off of the DRX layer gives rise to the high wear rate. Nevertheless, whether cracks initiate within the hcp/bcc interfaces need further clarification with more in-depth investigations in co-deformation of soft/hard phases.

4. Conclusions

In this work, tribo-induced surface deformation mechanisms are uncovered to play a paramount role in both the hcp and duplex Mg–Li alloys against friction and wear. The low friction and wear rate is intimately related to the stable nanograined tribo-layer through rapid grain refinement of the hcp grains at the initial stage of sliding. Peeling-off of the brittle fine-grained DRX layer is the primary reason for the poor wear resistance of the duplex Mg–Li alloy. Taking into account the tribo-induced surface deformation mechanisms, we are now focused on developing ultra-light, wear resistant hcp Mg–Li alloys via surface nanostructuring.

Funding

This work was supported by National Natural Science Foundation of China (Grant No. 52001165, 51931003, 51971112 and 51225102); the National Key R&D Program of China (Grant No. 2017YFA0204403); Natural Science Foundation of Jiangsu Province of China (Grant No. BK20200475) and the Fundamental Research Funds for the Central Universities (No. 30921011215 and 30919011405).

Author statement

Yue Yang: Data curation, Methodology, Investigation, Writing - Original Draft.

Ao Meng: Methodology, Investigation.

Xiang Chen: Conceptualization, Investigation, Supervision, Writing-Reviewing and Editing, Project Administration, Funding Acquisition.

Yonghao Zhao: Supervision, Writing-Reviewing and Editing, Project Administration, Funding Acquisition.

Declaration of competing interest

The authors declare that they have no known competing financial interests or personal relationships that could have appeared to influence the work reported in this paper.

Data availability

Data will be made available on request.

Acknowledgements

Y.H. Zhao and X. Chen want to acknowledge scientific & technical assistance from Jiangsu Key Laboratory of Advanced Nanomaterials and Technologies, Nanjing University of Science and Technology. Dr. L. Gu is sincerely acknowledged for assistance with FIB experiments.

Appendix A. Supplementary data

Supplementary data to this article can be found online at https://doi.org/10.1016/j.wear.2022.204507.

References

[1] W. Xu, N. Birbilis, G. Sha, Y. Wang, J.E. Daniels, Y. Xiao, M. Ferry, A high-specific-strength and corrosion-resistant magnesium alloy, Nat. Mater. 14 (2015) 1229–1235, https://doi.org/10.1038/nmat4435.

[2] T. Xin, Y. Zhao, R. Mahjoub, J. Jiang, A. Yadav, K. Nomoto, R. Niu, S. Tang, F. Ji, Z. Quadir, D. Miskovic, J. Daniels, W. Xu, X. Liao, L.-Q. Chen, K. Hagihara, X. Li, S. Ringer, M. Ferry, Ultrahigh specific strength in a magnesium alloy strengthened by spinodal decomposition, Sci. Adv. 7 (2021), https://doi.org/10.1126/sciadv.abf3039 eabf3039.

[3] S. Tang, T. Xin, W. Xu, D. Miskovic, G. Sha, Z. Quadir, S. Ringer, K. Nomoto, N. Birbilis, M. Ferry, Precipitation strengthening in an ultralight magnesium alloy, Nat. Commun. 10 (2019) 1003, https://doi.org/10.1038/s41467-019-08954-z.

[4] T.W. Cain, J.P. Labukas, The development of β phase Mg-Li alloys for ultralight corrosion resistant applications, Npj Mater. Degrad. 4 (2020) 1–10, https://doi.org/10.1038/s41529-020-0121-2.

[5] T. Al-Samman, Comparative study of the deformation behavior of hexagonal magnesium–lithium alloys and a conventional magnesium AZ31 alloy, Acta Mater. 57 (2009) 2229–2242, https://doi.org/10.1016/j.actamat.2009.01.031.

[6] M. Lentz, M. Klaus, I.J. Beyerlein, M. Zecevic, W. Reimers, M. Knezevic, In situ X-ray diffraction and crystal plasticity modeling of the deformation behavior of extruded Mg-Li-(Al) alloys: an uncommon tension-compression asymmetry, Acta Mater. 86 (2015) 254–268, https://doi.org/10.1016/j.actamat.2014.12.003.

[7] D. Xie, Z. Lyu, M. Fan, H.B. Chew, P.K. Liaw, H. Bei, Z. Zhang, Y. Gao, Micromechanical origin of the enhanced ductility in twinless duplex Mg-Li alloy, Mater. Sci. Eng., A 815 (2021), 141305, https://doi.org/10.1016/j.msea.2021.141305.

[8] T.C. Xu, X.D. Peng, J. Qin, Y.F. Chen, Y. Yang, G.B. Wei, Dynamic recrystallization behavior of Mg-Li-Al-Nd duplex alloy during hot compression, J. Alloys Compd. 639 (2015) 79–88, https://doi.org/10.1016/j.jallcom.2015.03.144.

[9] C. Haug, F. Ruebeling, A. Kashiwar, P. Gumbsch, C. Kübel, C. Greiner, Early deformation mechanisms in the shear affected region underneath a copper sliding contact, Nat. Commun. 11 (2020) 839, https://doi.org/10.1038/s41467-020-14640-2.

[10] P.C. Machado, J.I. Pereira, A. Sinatora, Subsurface microstructural dynamic recrystallization in multiscale abrasive wear, Wear 486–487 (2021), 204111, https://doi.org/10.1016/j.wear.2021.204111.

[11] X. Chen, Z. Han, X. Li, K. Lu, Lowering coefficient of friction in Cu alloys with stable gradient nanostructures, Sci. Adv. 2 (2016), e1601942, https://doi.org/10.1126/sciadv.1601942.

[12] B.N. Sahoo, S.K. Panigrahi, Development of wear maps of in-situ TiC+TiB2 reinforced AZ91 Mg matrix composite with varying microstructural conditions, Tribol. Int. 135 (2019) 463–477, https://doi.org/10.1016/j.triboint.2019.02.029.
[13] C. Liang, C. Li, X.X. Lv, J. An, Correlation between friction-induced microstructural evolution, strain hardening in subsurface and tribological properties of AZ31 magnesium alloy, Wear 312 (2014) 29–39, https://doi.org/10.1016/j.wear.2014.02.001.
[14] T. Yagi, T. Hirayama, T. Matsuoka, H. Somekawa, Effect of alloying elements on nano-ordered wear property of magnesium alloys, Metall. Mater. Trans., A 48 (2017) 1366–1374, https://doi.org/10.1007/s11661-016-3906-8.
[15] K. Sikdar, S. Shekhar, K. Balani, Fretting wear of Mg-Li-Al based alloys, Wear 318 (2014) 177–187, https://doi.org/10.1016/j.wear.2014.06.012.
[16] X. Peng, W. Liu, G. Wu, H. Ji, W. Ding, Plastic deformation and heat treatment of Mg-Li alloys: a review, J. Mater. Sci. Technol. 99 (2022) 193–206, https://doi.org/10.1016/j.jmst.2021.04.072.
[17] A. Fischer, W. Dudzinski, B. Gleising, P. Stemmer, Analyzing Mild- and Ultra-mild Sliding Wear of Metallic Materials by Transmission Electron Microscopy, Germany, 2008. Reference to a chapter in an edited book:.
[18] S. Balachandran, Z. Zachariah, A. Fischer, D. Mayweg, M.A. Wimmer, D. Raabe, M. Herbig, Atomic scale origin of metal ion release from hip implant taper junctions, Adv. Sci. 7 (2020), 1903008, https://doi.org/10.1002/advs.201903008.
[19] S. Wei, H. Zhang, C. Tangpatjaroen, J. Tarnsangpradit, A.D. Usta, M. Eriten, J. H. Perepezko, I. Szlufarska, Wear-induced microstructural evolution of ultra-fine grained (UFGs) aluminum, Acta Mater. 209 (2021), 116787, https://doi.org/10.1016/j.actamat.2021.116787.
[20] X. Chen, R. Schneider, P. Gumbsch, C. Greiner, Microstructure evolution and deformation mechanisms during high rate and cryogenic sliding of copper, Acta Mater. 161 (2018) 138–149, https://doi.org/10.1016/j.actamat.2018.09.016.
[21] H.Q. Sun, Y.N. Shi, M.-X. Zhang, Sliding wear-induced microstructure evolution of nanocrystalline and coarse-grained AZ91D Mg alloy, Wear 266 (2009) 666–670, https://doi.org/10.1016/j.wear.2008.08.004.
[22] C. Liu, Z. Li, W. Lu, Y. Bao, W. Xia, X. Wu, H. Zhao, B. Gault, C. Liu, M. Herbig, A. Fischer, G. Dehm, G. Wu, D. Raabe, Reactive wear protection through strong and deformable oxide nanocomposite surfaces, Nat. Commun. 12 (2021) 5518, https://doi.org/10.1038/s41467-021-25778-y.
[23] X. Chen, Y. Ma, Y. Yang, A. Meng, Z.X. Han, Z. Han, Y.H. Zhao, Revealing tribo–oxidation mechanisms of the copper-WC system under high tribological loading, Scripta Mater. 204 (2021), 114142, https://doi.org/10.1016/j.scriptamat.2021.114142.
[24] L. Li, S. Wang, L. Xiao, X. Chen, K. Wei, H. Ning, Y. Yu, D. Yin, H. Zhou, Atomic-scale three-dimensional structural characterisation of twin interface in Mg alloys, Phil. Mag. Lett. 100 (2020) 392–401, https://doi.org/10.1080/09500839.2020.1774935.
[25] Q. Peng, Y. Sun, B. Ge, H. Fu, Q. Zu, X. Tang, J. Huang, Interactive contraction nanotwins-stacking faults strengthening mechanism of Mg alloys, Acta Mater. 169 (2019) 36–44, https://doi.org/10.1016/j.actamat.2019.02.040.
[26] X. Chen, Z. Han, X.Y. Li, K. Lu, Friction of stable gradient nano-grained metals, Scripta Mater. 185 (2020) 82–87, https://doi.org/10.1016/j.scriptamat.2020.04.041.
[27] J. Liu, X.T. Deng, L. Huang, Z.D. Wang, Friction and wear behavior of nano/ultrafine-grained and heterogeneous ultrafine-grained 18Cr-8Ni austenitic stainless steels, Tribol. Int. 152 (2020), 106520, https://doi.org/10.1016/j.triboint.2020.106520.
[28] Y. Yang, X. Chen, J. Nie, K. Wei, Q. Mao, F. Lu, Y. Zhao, Achieving ultra-strong Magnesium–lithium alloys by low-strain rotary swaging, Mater. Res. Lett. 9 (2021) 255–262, https://doi.org/10.1080/21663831.2021.1891150.
[29] Q. Han, Y. Kang, P.D. Hodgson, N. Stanford, Quantitative measurement of strain partitioning and slip systems in a dual-phase steel, Scripta Mater. 69 (2013) 13–16, https://doi.org/10.1016/j.scriptamat.2013.03.021.
[30] Y. Sun, R. Wang, J. Ren, C. Peng, Y. Feng, Hot deformation behavior of Mg-8Li-3Al-2Zn-0.2Zr alloy based on constitutive analysis, dynamic recrystallization kinetics, and processing map, Mech. Mater. 131 (2019) 158–168, https://doi.org/10.1016/j.mechmat.2019.02.005.
[31] Q.C. Zhang, X. Chen, Z. Han, Subsurface morphological pattern, microstructure and wear response of Cu and Cu-Al alloys subjected to unidirectional and reciprocating sliding, Wear 462–463 (2020), 203521, https://doi.org/10.1016/j.wear.2020.203521.
[32] X. Chen, Z. Han, K. Lu, Wear mechanism transition dominated by subsurface recrystallization structure in Cu-Al alloys, Wear 320 (2014) 41–50, https://doi.org/10.1016/j.wear.2014.08.010.